Laser pulse driven control of charge and spin order in the two-dimensional Kondo lattice

Benedikt Fauseweh[1,*] and Jian-Xin Zhu[1,2,†]

[1]*Theoretical Division, Los Alamos National Laboratory, Los Alamos, New Mexico 87545, USA*

[2]*Center for Integrated Nanotechnologies, Los Alamos National Laboratory, Los Alamos, New Mexico 87545, USA*

(Received 12 August 2020; revised 24 September 2020; accepted 28 September 2020; published 14 October 2020)

Fast and dynamical control of quantum phases is highly desired in the application of quantum phenomena in devices. On the experimental side, ultrafast laser pulses provide an ideal platform to induce femtosecond dynamics in a variety of materials. Here we show that a laser pulse driven heavy fermion system can be tuned to dynamically evolve into a phase, which is not present in equilibrium. Using the state-of-the-art time-dependent variational Monte Carlo method, we perform numerical simulations of realistic laser pulses applied to the Kondo lattice model. By tracking spin and charge degrees of freedom we identify a dynamical phase transition, within the partially Kondo screened phase, from a charge ordered into a metallic state, while preserving the spin order of the system. We propose using high-harmonic generation and nonequilibrium optical conductivity to identify the dynamical phase transition in an ultrafast experiment.

DOI: 10.1103/PhysRevB.102.165128

I. INTRODUCTION

Heavy fermion systems are one prototypical class of strongly correlated materials. The most important microscopic mechanism in these systems is the Kondo effect, which is determined by the strength of the local Kondo coupling. It can be tuned by conventional means, such as external or chemical pressure [1]. At the same time, the Kondo coupling also leads to an effective interaction, known as the Ruderman-Kittel-Kasuya-Yosida (RKKY) interaction, between the local moments mediated via the conduction band electrons. The interplay between localized magnetic moments and conduction electrons is the driver behind unconventional superconductivity, competing phases, and quantum criticality. As such, heavy fermion materials share commonalities with many other strongly correlated electron systems, such as cuprates and organic or iron-based superconductors.

Experimental advances in nonlinear optics and ultrafast spectroscopy allow for unprecedented access to nonequilibrium physics of these strongly correlated materials. By using these techniques, many new and exciting phenomena have been discovered in recent years, such as light-induced superconductivity in cuprates [2], the generation of Higgs and order parameter oscillations [3–6], and the dynamical coupling of ferroelectric and ferromagnetic order [7]. The search for new quantum phases, which can only be obtained by photoinduction, is an ongoing quest in modern solid state physics [8–10]. It is guided by the idea of tailoring specific properties of materials on demand, for applications in electronic devices.

Although much of the progress focuses on nanostructures, complex oxides, and oxide heterostructures (e.g., cuprates, manganites, and multiferroics), heavy fermion systems have been investigated in ultrafast experiments as well [11–13]. However theoretical understanding of the transient nonequilibrium dynamics in these systems is still scarce. Many experiments can be explained by an effective temperature model [13–15], which describes the local excitation by an instantaneous heating process. This approach is limited in describing the possible nonequilibrium phase transitions, because it is only sensitive to thermodynamic phases which are also present in equilibrium. Furthermore effective temperature models, by construction, are not able to describe quantum coherence effects, which are an important aspect for the coherent control of quantum matter.

Even away from the quantum critical region, i.e., within the quantum coherence regime, interesting physics emerges such as non-Fermi-liquid electronic excitations. The effects of optical pumping in this area are largely unexplored and offer a unique opportunity to investigate the ensuing many-body nonequilibrium dynamics. Here we use state-of-the-art numerical simulations to investigate the unitary time evolution of a driven Kondo system, by means of the time-dependent variational Monte Carlo method [16–26]. Specifically we investigate the two-dimensional Kondo lattice model, which is used to model heavy fermion physics, at quarter filling. Studies by equilibrium variational Monte Carlo [27] and dynamical mean-field theory [28,29] have confirmed the presence of a coexisting charge density and spin order in this system. A graphical representation of the ground state is given in Fig. 1(a). Coexisting charge and spin order has also been confirmed experimentally in rare-earth intermetallic compounds [30,31]. By shaking the ground state with a strong laser field, we investigate the stability of both order parameters depending on the pulse intensity. We show that a dynamical phase transition can be induced by the pulse, leading to a purely spin-ordered phase, with suppressed charge order. This phase is absent in the thermodynamic phase diagram, and therefore goes beyond the description

*fauseweh@lanl.gov

†jxzhu@lanl.gov

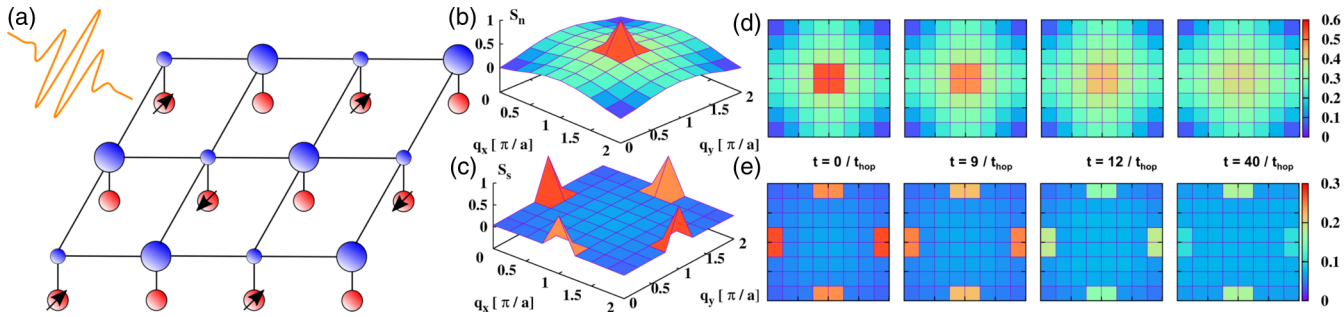

FIG. 1. Charge and spin order in the ground state and during the laser pulse excitation. (a) Graphical representation of the ground state of the Kondo lattice model for $J = 3t_{\rm hop}$ at quarter filling. Size of the blue circles is proportional to the charge density in the conduction band. Spin order is depicted for the f electrons. (b) Momentum dependence of the static charge structure factor in the ground state. (c) Momentum dependence of the static spin structure factor in the ground state. (d) Charge structure factor time evolution for a pulse with peak amplitude $A_0 = 0.75$. (e) Spin structure factor time evolution for a pulse with peak amplitude $A_0 = 0.75$.

by an effective temperature model. Analysis of the underlying many-body dynamics shows that the transient electronic structure is strongly modified during the pulse, leading to a dynamical closure of the charge gap. Finally we suggest using optical conductivity and high-harmonic generation (HHG) spectroscopy as an experimental signature for the dynamical phase transition.

II. MODEL AND METHOD

The Kondo lattice model is defined by

$$\mathcal{H} = -t_{\rm hop} \sum_{\langle i,j\rangle,\sigma} (c^\dagger_{i\sigma} c_{j\sigma} + \text{H.c.}) + J \sum_i \mathbf{s}_i \cdot \mathbf{S}_i. \qquad (1)$$

The first term is the kinetic energy of the conduction electrons; the second term is the Kondo coupling of the conduction band electron spin $\mathbf{s}_i$ to the local $SU(2)$ moments $\mathbf{S}_i$ of the f electrons. In the following we use $e = c = \hbar = a = 1$, where a is the lattice spacing. Unless otherwise noted, we use the hopping $t_{\rm hop}$ as our unit of energy and $1/t_{\rm hop}$ as our unit of time.

Although much attention has been given to electron filling factors close to the half-filled case in the recent literature [28,32], we are focusing on the quarter filled case for $J = 3t_{\rm hop}$, where the electron density is given by $n = 1/2$. Note that it was shown that also for other parameters charge and magnetic order coexist [27,28,33], although the exact ground state phase diagram is still a matter of debate. Since our excitation mechanism does not rely on a specific geometric form for the charge or spin sector, we expect that our results also carry over to other parameter regimes as well.

We include a time-dependent EM field by the well established Peierls substitution [34–36]

$$t_{\rm hop} \to t_{\rm hop} e^{i\mathbf{A}(t)(\mathbf{r}_i - \mathbf{r}_j)}, \qquad (2)$$

where $\mathbf{A}(t)$ is the time-dependent vector potential.

We choose a diagonal polarization $\mathbf{A}(t) = A(t)(\mathbf{e}_x + \mathbf{e}_y)$ and parametrize the pulse according to $A(t) = A_0 \exp[-(t - t_c)^2/(2t_d^2)] \cos(\omega t)$. Here A_0 is the pulse amplitude, t_c the center, t_d the width, and ω the frequency of the pulse.

Note that by considering the Kondo lattice model we disregard a possible charge degree of freedom for the f electrons. In the original Anderson model, part of the f-electron spectral weight is mobile in the paramagnetic phase. The electromagnetic field would couple to this spectral weight near the Fermi energy. In the antiferromagnetically ordered phase we neglect this contribution.

Method

We use variational Monte Carlo (VMC) and its time-dependent version (tVMC) to compute ground state and time-evolved properties of the system, respectively. In our simulations we choose a square lattice of size 8×8 with periodic (antiperiodic) boundary conditions in the x (y) direction to fulfill the closed shell condition in the noninteracting case. Note that larger systems can be simulated for pure ground state properties. The time evolution however demands much more computational effort and is therefore the restricting factor.

The variational wave function we employ in VMC and tVMC is given by

$$|\Psi\rangle = P_G P_J |\phi\rangle, \quad |\phi\rangle = \left(\sum_{\alpha,\beta=\langle c,f\rangle} \sum_{i,j}^{N_s} f_{ij} \alpha^\dagger_{i\uparrow} \beta^\dagger_{j\downarrow} \right)^{N_e/2} |0\rangle. \qquad (3)$$

Here $|\phi\rangle$ is the Pfaffian wave function for conduction band and f electrons. The variational parameters in the Pfaffian wave function are given by the f_{ij}. The correlation factors P_G and P_J are of Gutzwiller and Jastrow type. For f electrons the Gutzwiller factor is the only relevant correlation factor, as it permits only single occupancy of the lattice sites, effectively casting the f degrees of freedom to a single spin-1/2, as relevant for the Kondo lattice model. The variational parameters are subject to a 2×2 sublattice structure [37]. To obtain the ground state we optimize the variational parameters using stochastic reconfiguration [38].

We employ the time-dependent variational principle onto the wave function to compute the time dependence of the variational parameters [39]. Specifically, we minimize the norm

$$\min_\alpha \left\| \left(1 - \frac{|\Psi\rangle\langle\Psi|}{\langle\Psi|\Psi\rangle}\right) \left(i \frac{d}{dt} |\Psi\rangle - \mathcal{H}|\Psi\rangle\right) \right\|, \qquad (4)$$

depending on the variational parameters α. This leads to the equation of motion

$$\frac{d\alpha}{dt} = -i(S)^{-1}\mathbf{g}, \tag{5}$$

where the S matrix and the vector $\mathbf{g}$ are functions of the energy as well as the derivative of $|\Psi\rangle$ with respect to the variational parameters. These quantities are computed using Monte Carlo sampling and Eq. (5) is solved using the MINRES-QLP algorithm [40] at each time step. Note that the tVMC approach has been benchmarked for fermionic systems against exact diagonalization in Ref. [18]. For details on the tVMC approach we refer the reader to Supplemental Material S1 [41].

III. RESULTS

The pulse parameters that we use are $A_0 = 0.5, 0.75, 1.0$; $\omega = 1.0t_{\text{hop}}$; $t_c = 15.0/t_{\text{hop}}$; and $t_d = 5.0/t_{\text{hop}}$. Note that these parameters are well within the reach of experimental setups. Taking the lattice spacing from $CeRhIn_5$, in which a coexisting charge density wave with antiferromagnetic ordering was induced by a magnetic field [42], $a = 0.4656$ nm [43], and assuming a typical bandwidth of about 1 eV for the conduction electrons leads to a hopping parameter of $t_{\text{hop}} = 0.125$ eV. Therefore the laser pulse frequency corresponds to 30 THz and the pulse width to 52 fs. The laser amplitude corresponds to a maximal electric field $E_0 \propto 26.6$ MV/cm. The energy that is deposited in a single layer by the laser is computed in Supplemental Material S2 [41]. Note that a choice of a smaller laser field frequency (e.g., in the regime of typical Kondo coherence energy) does not affect the conclusion.

A. Ground state properties at quarter filling

To characterize the ground state properties, we compute the spin and charge structure factors

$$S_S(\mathbf{q}) = \frac{1}{N_S}\sum_{i,j}\langle \mathbf{S}_i \cdot \mathbf{S}_j\rangle e^{i\mathbf{q}(\mathbf{r}_i-\mathbf{r}_j)}, \tag{6}$$

$$S_N(\mathbf{q}) = \frac{1}{N_S}\sum_{i,j}\langle (n_i - \langle n_i\rangle)(n_j - \langle n_j\rangle)\rangle e^{i\mathbf{q}(\mathbf{r}_i-\mathbf{r}_j)}, \tag{7}$$

where $\mathbf{S}_i$ denotes the local f-electron spin. They are shown in Figs. 1(b) and 1(c), respectively. We see strong peaks in the spin structure factor at $q = (0, \pi)$ and $q = (\pi, 0)$ [and equivalently at $q = (\pi, 2\pi)$ and $q = (2\pi, \pi)$], indicative of antiferromagnetic order, which is not of the conventional Néel type. Note that the peak height is slightly different for x and y direction, due to the different boundary conditions; see also the methods section. The charge structure factor shows a single strong peak at $q = (\pi, \pi)$, corresponding to a checkerboard type charge order. The unusual spin order leads to a magnetic unit cell, which is 4 times larger than the geometric unit cell. This ground state has been confirmed in [27–29]. The charge-ordered phase is an insulator, with a charge gap $\Delta_c \approx 0.4t_{\text{hop}}$ at $J = 3t_{\text{hop}}$ [27]. Note that this coexistence of charge and spin order is specific to the 1/4-filled region. The real-space dynamical mean field theory calculations have shown coexistence of incommensurate spin density wave and charge density wave phases for other doping values and interaction parameters [28].

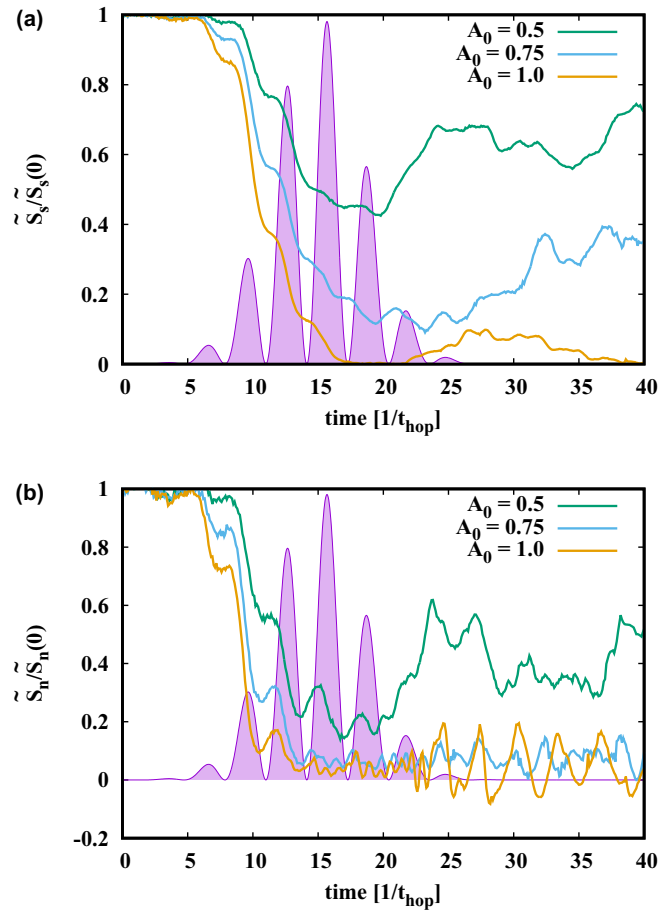

FIG. 2. Time evolution of the spin and charge structure factor. (a) Comparison of the peaks in the spin structure factor for different laser pulse amplitudes. The shaded background is proportional to the squared pulse profile. (b) Comparison of the peak in the charge structure factor for the same parameters as in (a). See methods section for the definitions of the relative peak height $\tilde{S}_s$ and $\tilde{S}_n$.

B. Laser excitation

The system is perturbed with a laser pulse and we track the dynamics in the spin and charge sectors. An overview of the time evolution of the spin and charge structure factors is shown in Figs. 1(d) and 1(e), for a pulse amplitude of $A_0 = 0.75$. As the pulse progresses, the peaks in the charge and spin order are strongly suppressed by the pump pulse. The remaining Brillouin zone remains largely unaffected, indicating that the pulse primarily modifies the dominating charge and magnetic fluctuations. To make more quantitative statements the time dependence of the peaks is investigated. We define the peak heights as

$$\tilde{S}_s(t) = \frac{S_s((0,\pi),t) + S_s((\pi,0),t)}{2} - \underset{q\in\tilde{q}}{\text{mean}}[S_s(\mathbf{q},t)], \tag{8}$$

$$\tilde{S}_n(t) = S_n((\pi,\pi),t) - \underset{q\in\tilde{q}}{\text{mean}}[S_n(\mathbf{q},t)], \tag{9}$$

where $\tilde{q}$ are all momentum space points in direct neighborhood to the peak positions in the Brillouin zone. We compare the effect of different pulse amplitudes. The results are given in Fig. 2.

Our first observation is that the pulse suppresses both peaks during the time evolution. Increasing the pulse amplitude in general leads to a stronger suppression. The time domain in which the peak height shows the strongest decrease coincides with the maxima in the pulse line shape (see shaded regions in Fig. 2), reflecting the influence of the laser pulse onto the electronic and magnetic structure. Depending on the response of the system, we can distinguish three different regimes: (1) For weak pulses, $A_0 = 0.5$, both charge and spin order are suppressed but stay finite after the pulse. We see slow oscillations in the time domain, even after the pulse has ended. Note that low-intensity high-frequency oscillations are expected on top of the overall dynamics due to the finite system size. (2) In the intermediate regime at $A_0 = 0.75$ the charge order in Fig. 2(b) is strongly suppressed and on average close to zero, while the spin order, Fig. 2(a), is still larger than 30% of the ground state value. (3) Further increasing the intensity to $A_0 = 1.0$ also suppresses the spin order, while the charge order shows stronger oscillations but with an average close to zero.

These results are to be contrasted with the thermal phase diagram [27], in which thermal fluctuation first suppress spin order, while the critical temperature for the charge order is much higher. The direct coupling of the EM field to the charge is a possible explanation for this behavior: while the spin degrees of freedom of the f electrons are only indirectly affected through the Kondo coupling, the conduction band electrons react directly to laser pulse. In contrast thermal fluctuations do not distinguish between charge and spin sector. Hence the naive expectation that the laser pulse simply heats the system does not hold in this case.

Note that the suppression of the peaks in the charge and spin sector correspond to a suppression of the order parameters in the thermodynamic limit. Thus our simulations directly hint at a dynamic phase transition in time, controllable by the pulse amplitude.

To get a deeper microscopic understanding of the dynamics, we also calculated the time evolution of the double occupancy and the momentum distribution,

$$n_{\mathbf{q}}(t) = \frac{1}{2N_s} \sum_{i,j,\sigma} \langle c^{\dagger}_{i\sigma} c_{j\sigma} \rangle(t) e^{i\mathbf{q}(\mathbf{r}_i - \mathbf{r}_j)}. \tag{10}$$

The double occupancy, shown in Fig. 3, displays a strong oscillatory behavior during the pulse duration. While for the lowest pump amplitude the double occupancy almost recovers to its equilibrium value, higher pump amplitudes lead to a significant change and increase. Note that the value of the double occupancy for the metallic, noninteracting system is $1/16 = 0.0625$. Thus, judging only from the observed time evolution of the double occupancy, the system becomes more metallic for stronger pump pulses.

This observation is supported by the time evolution of the momentum distribution, shown in Fig. 4. In equilibrium, Fig. 4(a), the momentum distribution has a smooth dependence on momentum, indicative of an insulating behavior. During the pulse evolution the momentum distribution stays smooth as a function of momentum, but weight is transferred away from the center of the Brillouin zone to the outer

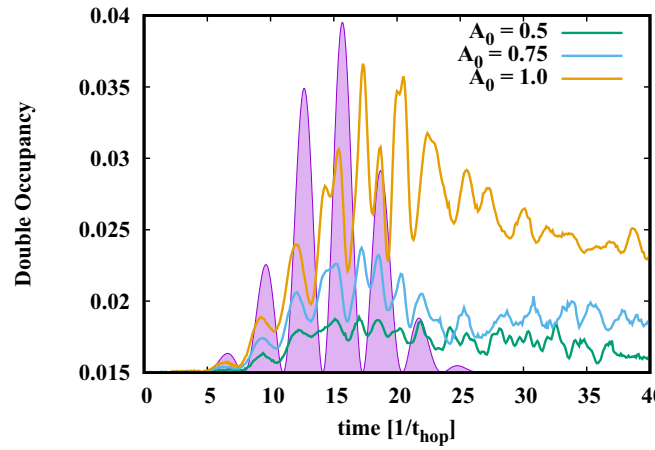

FIG. 3. Double occupancy of the conduction electrons during and after the laser pulse. Comparison for different laser pulse amplitudes. The shaded background is proportional to the squared pulse profile.

regions; see Fig. 4(b). This corresponds to the creation of free charge carriers and thus a breakdown of the charge insulator.

To further verify the dynamical melting of the charge insulator we investigate the small momentum dependence of the charge structure factor $S_n(\mathbf{q})$ in Supplemental Material S3 [41]. We observe a change of the scaling from quadratic to linear, which is also observed for the equilibrium Mott

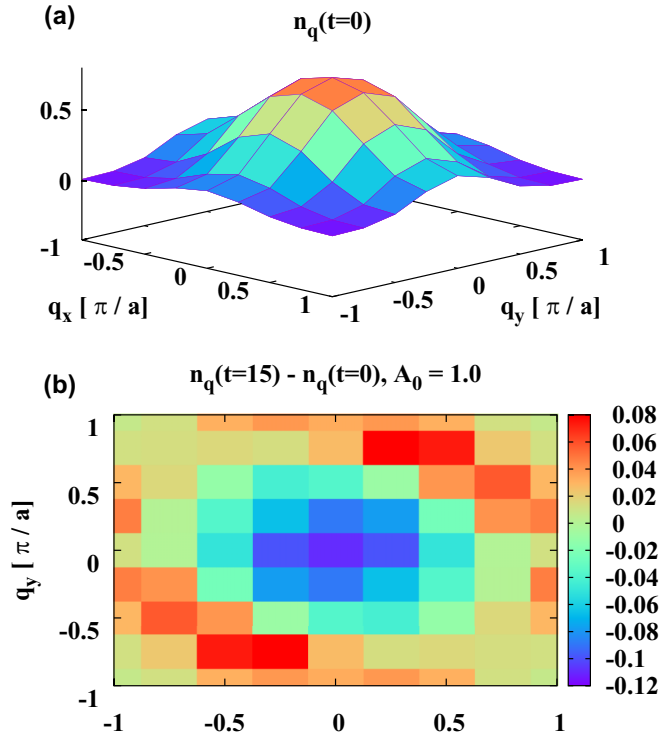

FIG. 4. Momentum distribution in the ground state and during the laser pulse. (a) Momentum distribution of the conduction electrons in the ground state of the Kondo lattice model for $J = 3t$ and quarter filling. (b) Difference between the momentum distribution in the ground state and at $t = 15$ for a laser pulse with $A_0 = 1.0$.

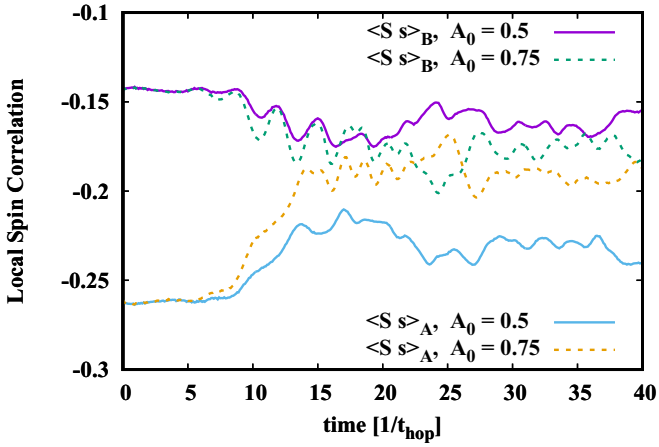

FIG. 5. Time evolution of the local spin correlation $\langle \mathbf{S}^c \cdot \mathbf{S}^f \rangle$. Comparison of charge-rich sites A and charge-poor sites B. Laser intensities are $A_0 = 0.5$ and $A_0 = 0.75$.

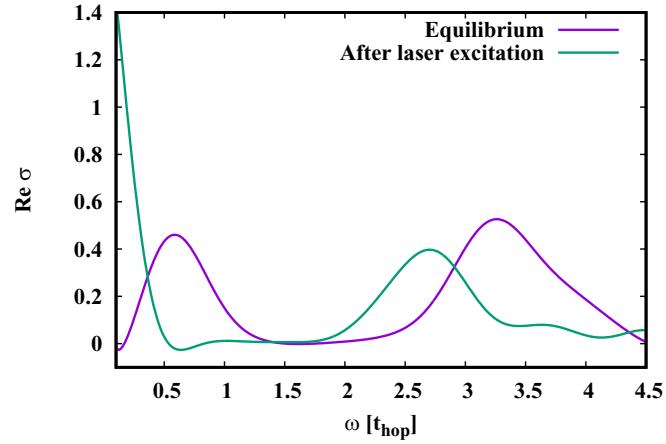

FIG. 6. Real part of the optical conductivity in and out of equilibrium. Computed from a probe pulse in equilibrium and after a pump pulse with amplitude $A_0 = 1.0$. Probe pulse parameters are $A_0 = 0.05$, $\omega = 2.0\,t_{\rm hop}$, and $t_d = 1.0/t_{\rm hop}$ at quarter filling. The time delay between pump and probe pulse is $\Delta t = 20/t_{\rm hop}$.

transition in the Hubbard model [44–46]. We conclude that the dynamical phase transition is accompanied by a meltdown of the insulating state.

C. Dynamical Kondo screening

The local Kondo singlet formation plays a critical role in the stabilization of the charge-ordered phase [27]. Specifically the unusual spin ordering wave vector allows for a stronger Kondo effect on the charge-rich sites, while the charge-poor sites exhibit magnetic ordering, as seen in Fig. 1. An estimate for the competition between magnetic order and the Kondo effect is given in Supplemental Material S4 [41]. This raises the interesting question of how the interplay between the Kondo screening and the magnetic sublattice is affected by the laser pulse. We investigate the spin correlations $\langle \mathbf{S}_i \cdot \mathbf{s}_i \rangle$, which is a measure for the local singlet formation, between the conduction band electrons and the magnetic moments on the charge-rich A and charge-poor B sublattice as function of time during laser irradiation. The results are shown in Fig. 5. We observe that the effect of the laser pulse is different for the sublattices: While for the A sites the local correlation is reduced, it is enhanced for the B sites. The effect is not as pronounced for the weak pulse $A_0 = 0.5$. However, already for the intermediate pulse $A_0 = 0.75$, it is strong enough to level out the differences between A and B sublattices on average. A comparison to the time evolution of the charge structure factor in Fig. 2(b) reveals the connection to the time evolution of the charge order. Due to the laser excitation, a charge balance is established and the previously charge-rich sites are depleted and consequently the local spin correlation is reduced. The opposite happens for the previously charge-poor sites. Note that the laser pulse does not break the local singlet formation. It rather dynamically modifies the charge background so that the overall spin singlet formation is affected only weakly.

D. Pump-probe optical conductivity

To observe the dynamics after a strong pump pulse, a probe pulse is applied after a time delay Δt. In our simulation we explicitly simulate the effect of the probe pulse and compute the resulting optical conductivity with a procedure developed in Ref. [47]; see also Supplemental Material S5 [41]. Note that the pump pulse parameters are chosen such that we have a maximal resolution for frequencies $\omega = 0$ to $\omega = 5t_{\rm hop}$, capturing the complete electronic bandwidth. We compare the nonequilibrium results with the optical conductivity in equilibrium. The results are shown in Fig. 6.

In agreement with previous results, the ground state is insulating and shows two strong absorption peaks at $\omega \approx 0.6t_{\rm hop}$ and at $\omega \approx 3.3t_{\rm hop}$. Drastic changes occur after a pump pulse: (1) A finite Drude peak develops at $\omega = 0$, indicative of a metallic state. (2) The absorbtion peak at $\omega \approx 0.6t_{\rm hop}$ vanishes completely. (3) The peak at $\omega \approx 3.3t_{\rm hop}$ shifts toward lower energies. A possible microscopic explanation for the complete reorganization of the electronic response is the dynamical phase transition from an insulating to a conducting state. Thus not only static properties, such as the structure factors, are strongly affected by the pump pulse, but also typical excitation spectra which can be related uniquely to the underlying phases by means of their elementary excitations. Note that the photoinduced insulator-metal transition originates from the collapse of the charge order in the Kondo coherence regime, while the spin order as well as the Kondo singlet formation are robust against the laser pulse.

E. High-harmonic generation

The effect of the single pump pulse can be used to obtain insight into the nonequilibrium dynamics of the system. We therefore compute the charge current, which is induced by the pump pulse. The result is shown in Fig. 7(a). For weak pump fluence, $A_0 = 0.5$, the response of the system is primarily linear in the EM field, while we see clear nonlinearities in the current for stronger fluence, e.g., $A_0 = 1.0$. We traced these nonlinearities back to the generation of higher harmonics, which can be observed in the current emission spectroscopy,

$$\left| \mathrm{FT}\left[\frac{dJ_c(t)}{dt} \right] \right|^2 (\omega), \tag{11}$$

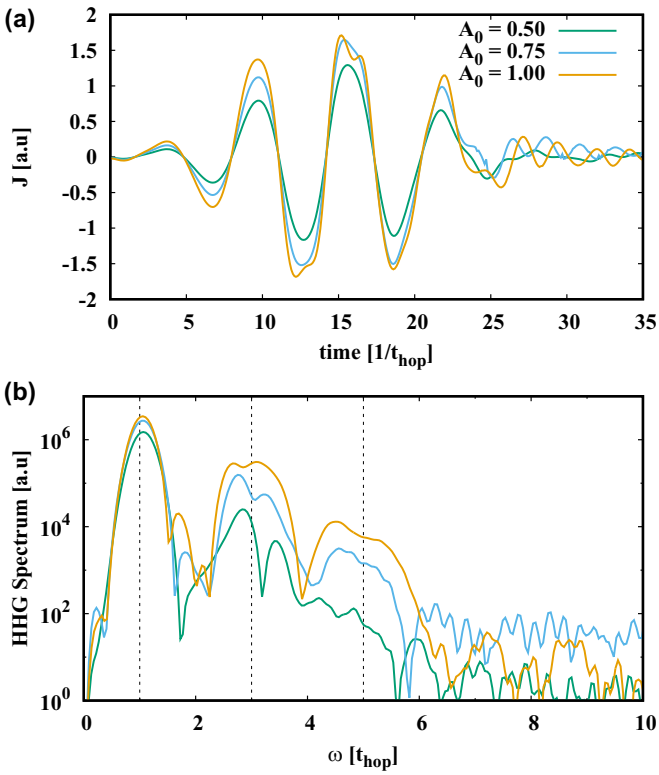

FIG. 7. High-harmonic generation during the laser pulse. (a) Induced current for different laser pulse amplitudes. (b) High-harmonic generation spectrum for the same currents as in (a). Vertical lines show the first, third, and fifth harmonic position, respectively.

where FT denotes the Fourier transformation of the dipole acceleration $dJ_c(t)/dt$ along the diagonal with a window function; see Supplemental Material S6 [41]. We observe that odd harmonics are generated by the pump pulse in the system; see Fig. 7(b). It is expected that photoexcited charge carriers create a nonlinear optical response in solids [48,49]. The lack of even harmonics is a consequence of the inversion symmetry of the system [50,51]. While the fundamental harmonic is only weakly dependent on the pulse amplitude, higher harmonics show a strong dependence on the pulse amplitude. In the third harmonic we see an increase in the signal by more than one order of magnitude by doubling the laser amplitude from $A_0 = 0.5$ to $A_0 = 1.0$. For low pulse intensities, the third harmonic shows a clear two peak structure. It is known that in noninteracting multiorbital systems the electronic band structure can have a strong effect on the HHG spectra [52,53]. By contrast we attribute the two-peak structure in our case to the strong correlations in the system, which leads to the formation of charge order. This is in accordance with the broadening of the signal upon dynamical closing of the charge gap due to the pump pulse. We checked that such a double-peak structure is absent in the noninteracting system, i.e., for $J = 0$ without charge order. The effect in the fifth harmonic is even stronger: in the weak-pulse regime the fifth harmonic cannot be distinguished from the background, while it shows a strong peak once the charge and spin order are suppressed.

In a simple model the creation of high harmonics is a two-step process: First charge carriers are excited from the ground state to a conduction band. In the second step they are accelerated by the finite electric field, leading to an intraband current. Due to the strong field, electrons are Bragg scattered at the zone boundaries, leading to Bloch oscillations and radiation of photons with odd multiples of the laser driving frequency. In the noninteracting case, the cutoff frequency for the appearance of high harmonics scales linearly with the maximal amplitude of the laser field [54] but in interacting systems or in the presence of disorder, the HHG signal can be strongly modified [55,56]. In our case, the strong change in the electronic state, i.e., the melting of the charge order due to the laser pulse, leads to a significant enhancement of the HHG spectrum.

We conclude that there is a strong feedback effect on the high harmonics depending on the internal dynamics of the charge and spin orders. Besides measurements of optical conductivity, this could serve as an experimental indicator to identify the different dynamical regimes induced by the pump pulse.

IV. DISCUSSION

In this paper we have investigated the dynamics of the spin and charge degrees of freedom in the 2D Kondo lattice model driven by a strong laser pump field. The interplay between charge density and spin order can be strongly influenced by the light field, allowing us to dynamically manipulate the basic characteristics of the system. By tuning the laser intensity, we have shown that charge fluctuations can be dynamically suppressed in favor of spin order, effectively inverting the temperature phase diagram of the model and allowing us to modify the system with an additional independent parameter besides pure heating. The dynamical phase transition is accompanied by a meltdown of the charge gap, as evidenced by microscopic observables such as double occupancy and momentum distribution. By computing the time evolution of the local spin correlation we show that the Kondo effect shows an intricate connection to the time evolution of the charge structure. Most importantly the laser does not break the Kondo singlets but establishes a uniform charge background to which the local moments couple. Finally we have demonstrated that time-resolved optical conductivity and high-harmonic generation can be used as an experimental characterization tool for the dynamical phase transition.

Our work provides a mechanism for the ultrafast manipulation of coexisting charge and spin orders in Kondo systems, offering a way to explore transient and hidden phases, which cannot be attained by conventional methods, such as temperature or pressure. In the spirit of "quantum phases on demand" [57], this provides a theoretical approach for the application of tailored ultrashort laser pulses to strongly correlated materials.

Many questions are raised by our results, which are to be explored. An important basic condition for our study is the assumption that the charge character of the local moments can be neglected. It is an interesting problem to relax this condition in order to directly study the laser-induced breaking down of the Kondo singlets, e.g., by explicitly considering the Anderson lattice model. While the system we investigated exhibits a coexisting charge and spin order, heavy fermion systems also display unconventional superconductivity and

antiferromagnetism [58–60], and the coexistence of both, which could be tuned in a similar fashion. It is important to note that a phase transition is hard to distinguish from a crossover in a nonequilibrium setup and that there is no consensus in the literature on how to define a nonequilibrium phase transition. While the notion of nonanalytical points in the Loschmidt echo [61] applies in the thermodynamic limit, there are also indications that a fundamental change in the excitation spectrum indicates a transition to a new phase [62]. Here we use the time dependence of properties, such as the structure factors, as well as the change in the quasiparticle spectrum in the optical conductivity to observe a strong change in the physics of the system, which is similar to what is observed in an equilibrium phase transition. Still one has to be cautious with this interpretation because an exact transition point cannot be deduced from our results. An important open question is the timescale for the induced dynamical phase transition, for which the effect of electronic relaxation, quantum criticality, and impact of coupling to lattice phonons are of interest.

ACKNOWLEDGMENTS

We thank Chen-Yen Lai and Stuart Trugman for fruitful discussions. This work was supported by the US DOE NNSA under Contract No. 89233218CNA000001 via the LANL LDRD Program. It was supported in part by the Center for Integrated Nanotechnologies, a US DOE Office of Basic Energy Sciences user facility, in partnership with the LANL Institutional Computing Program for computational resources.

[1] S. Wirth and F. Steglich, Exploring heavy fermions from macroscopic to microscopic length scales, Nat. Rev. Mater. **1**, 16051 (2016).

[2] D. Fausti, R. I. Tobey, N. Dean, S. Kaiser, A. Dienst, M. C. Hoffmann, S. Pyon, T. Takayama, H. Takagi, and A. Cavalleri, Light-induced superconductivity in a stripe-ordered cuprate, Science **331**, 189 (2011).

[3] R. Matsunaga, Y. I. Hamada, K. Makise, Y. Uzawa, H. Terai, Z. Wang, and R. Shimano, Higgs Amplitude Mode in the BCS Superconductors $Nb_{1-x}Ti_xN$ Induced by Terahertz Pulse Excitation, Phys. Rev. Lett. **111**, 057002 (2013).

[4] D. Werdehausen, T. Takayama, M. Höppner, G. Albrecht, A. W. Rost, Y. Lu, D. Manske, H. Takagi, and S. Kaiser, Coherent order parameter oscillations in the ground state of the excitonic insulator Ta_2NiSe_5, Sci. Adv. **4**, eaap8652 (2018).

[5] H. Krull, N. Bittner, G. S. Uhrig, D. Manske, and A. P. Schnyder, Coupling of Higgs and Leggett modes in nonequilibrium superconductors, Nat. Commun. **7**, 11921 (2016).

[6] L. Schwarz, B. Fauseweh, N. Tsuji, N. Cheng, N. Bittner, H. Krull, M. Berciu, G. S. Uhrig, A. P. Schnyder, S. Kaiser, and D. Manske, Classification and characterization of nonequilibrium Higgs modes in unconventional superconductors, Nat. Commun. **11**, 287 (2020).

[7] Y. M. Sheu, S. A. Trugman, L. Yan, Q. X. Jia, A. J. Taylor, and R. P. Prasankumar, Using ultrashort optical pulses to couple ferroelectric and ferromagnetic order in an oxide heterostructure, Nat. Commun. **5**, 5832 (2014).

[8] D. M. Kennes, E. Y. Wilner, D. R. Reichman, and A. J. Millis, Transient superconductivity from electronic squeezing of optically pumped phonons, Nat. Phys. **13**, 479 (2017).

[9] X. Yang, C. Vaswani, C. Sundahl, M. Mootz, P. Gagel, L. Luo, J. H. Kang, P. P. Orth, I. E. Perakis, C. B. Eom, and J. Wang, Terahertz-light quantum tuning of a metastable emergent phase hidden by superconductivity, Nat. Mater. **17**, 586 (2018).

[10] F. Giorgianni, T. Cea, C. Vicario, C. P. Hauri, W. K. Withanage, X. Xi, and L. Benfatto, Leggett mode controlled by light pulses, Nat. Phys. **15**, 341 (2019).

[11] C. Wetli, S. Pal, J. Kroha, K. Kliemt, C. Krellner, O. Stockert, H. van Löhneysen, and M. Fiebig, Time-resolved collapse and revival of the Kondo state near a quantum phase transition, Nat. Phys. **14**, 1103 (2018).

[12] D. Talbayev, K. S. Burch, E. E. M. Chia, S. A. Trugman, J.-X. Zhu, E. D. Bauer, J. A. Kennison, J. N. Mitchell, J. D. Thompson, J. L. Sarrao, and A. J. Taylor, Hybridization and Superconducting Gaps in the Heavy-Fermion Superconductor $PuCoGa_5$ Probed via the Dynamics of Photoinduced Quasiparticles, Phys. Rev. Lett. **104**, 227002 (2010).

[13] D. Leuenberger, J. A. Sobota, S.-L. Yang, H. Pfau, D.-J. Kim, S.-K. Mo, Z. Fisk, P. S. Kirchmann, and Z.-X. Shen, Dehybridization of f and d states in the heavy-fermion system $YbRh_2Si_2$, Phys. Rev. B **97**, 165108 (2018).

[14] L. Perfetti, P. A. Loukakos, M. Lisowski, U. Bovensiepen, H. Eisaki, and M. Wolf, Ultrafast Electron Relaxation in Superconducting $Bi_2Sr_2CaCu_2O_{8+\delta}$ by Time-Resolved Photoelectron Spectroscopy, Phys. Rev. Lett. **99**, 197001 (2007).

[15] J. Tao, R. P. Prasankumar, E. E. M. Chia, A. J. Taylor, and J.-X. Zhu, Theory of ultrafast quasiparticle dynamics in high-temperature superconductors: The dependence on pump fluence, Phys. Rev. B **85**, 144302 (2012).

[16] G. Carleo, F. Becca, M. Schiró, and M. Fabrizio, Localization and glassy dynamics of many-body quantum systems, Sci. Rep. **2**, 243 (2012).

[17] G. Carleo, F. Becca, L. Sanchez-Palencia, S. Sorella, and M. Fabrizio, Light-cone effect and supersonic correlations in one- and two-dimensional bosonic superfluids, Phys. Rev. A **89**, 031602 (2014).

[18] K. Ido, T. Ohgoe, and M. Imada, Time-dependent many-variable variational Monte Carlo method for nonequilibrium strongly correlated electron systems, Phys. Rev. B **92**, 245106 (2015).

[19] K. Ido, T. Ohgoe, and M. Imada, Correlation-induced superconductivity dynamically stabilized and enhanced by laser irradiation, Sci. Adv. **3**, e1700718 (2017).

[20] G. Carleo and M. Troyer, Solving the quantum many-body problem with artificial neural networks, Science **355**, 602 (2017).

[21] G. Carleo, Y. Nomura, and M. Imada, Constructing exact representations of quantum many-body systems with deep neural networks, Nat. Commun. **9**, 5322 (2018).

[22] L. Cevolani, G. Carleo, and L. Sanchez-Palencia, Protected quasilocality in quantum systems with long-range interactions, Phys. Rev. A **92**, 041603 (2015).

[23] G. Fabiani and J. H. Mentink, Investigating ultrafast quantum magnetism with machine learning, SciPost Phys. **7**, 004 (2019).
[24] Y. Nomura, A. S. Darmawan, Y. Yamaji, and M. Imada, Restricted Boltzmann machine learning for solving strongly correlated quantum systems, Phys. Rev. B **96**, 205152 (2017).
[25] M. Schmitt and M. Heyl, Quantum Many-Body Dynamics in Two Dimensions with Artificial Neural Networks, Phys. Rev. Lett. **125**, 100503 (2020).
[26] I. López-Gutiérrez and C. B. Mendl, Real-time evolution with neural-network quantum states, arXiv:1912.08831.
[27] T. Misawa, J. Yoshitake, and Y. Motome, Charge Order in a Two-Dimensional Kondo Lattice Model, Phys. Rev. Lett. **110**, 246401 (2013).
[28] R. Peters and N. Kawakami, Large and small Fermi-surface spin density waves in the Kondo lattice model, Phys. Rev. B **92**, 075103 (2015).
[29] R. Peters and N. Kawakami, Competition of striped magnetic order and partial Kondo screened state in the Kondo lattice model, Phys. Rev. B **96**, 115158 (2017).
[30] F. Galli, S. Ramakrishnan, T. Taniguchi, G. J. Nieuwenhuys, J. A. Mydosh, S. Geupel, J. Lüdecke, and S. van Smaalen, Charge-Density-Wave Transitions in the Local-Moment Magnet $Er_5Ir_4Si_{10}$, Phys. Rev. Lett. **85**, 158 (2000).
[31] K. K. Kolincio, M. Roman, M. J. Winiarski, J. Strychalska-Nowak, and T. Klimczuk, Magnetism and charge density waves in $R\mathrm{NiC}_2$(R = Ce,Pr,Nd), Phys. Rev. B **95**, 235156 (2017).
[32] B. Lenz, R. Gezzi, and S. R. Manmana, Variational cluster approach to superconductivity and magnetism in the Kondo lattice model, Phys. Rev. B **96**, 155119 (2017).
[33] J. Otsuki, H. Kusunose, and Y. Kuramoto, The Kondo lattice model in infinite dimensions: II. Static susceptibilities and phase diagram, J. Phys. Soc. Jpn. **78**, 034719 (2009).
[34] M. Claassen, H.-C. Jiang, B. Moritz, and T. P. Devereaux, Dynamical time-reversal symmetry breaking and photo-induced chiral spin liquids in frustrated Mott insulators, Nat. Commun. **8**, 1192 (2017).
[35] T. Konstantinova, J. D. Rameau, A. H. Reid, O. Abdurazakov, L. Wu, R. Li, X. Shen, G. Gu, Y. Huang, L. Rettig, I. Avigo, M. Ligges, J. K. Freericks, A. F. Kemper, H. A. Dürr, U. Bovensiepen, P. D. Johnson, X. Wang, and Y. Zhu, Nonequilibrium electron and lattice dynamics of strongly correlated $Bi_2Sr_2CaCu_2O_{8+\delta}$ single crystals, Sci. Adv. **4**, eaap7427 (2018).
[36] W. Shen, Y. Ge, A. Y. Liu, H. R. Krishnamurthy, T. P. Devereaux, and J. K. Freericks, Nonequilibrium "Melting" of a Charge Density Wave Insulator via an Ultrafast Laser Pulse, Phys. Rev. Lett. **112**, 176404 (2014).
[37] T. Misawa, S. Morita, K. Yoshimi, M. Kawamura, Y. Motoyama, K. Ido, T. Ohgoe, M. Imada, and T. Kato, mVMC—Open-source software for many-variable variational Monte Carlo method, Comput. Phys. Commun. **235**, 447 (2019).
[38] S. Sorella, Generalized Lanczos algorithm for variational quantum Monte Carlo, Phys. Rev. B **64**, 024512 (2001).
[39] J. Haegeman, T. J. Osborne, and F. Verstraete, Post-matrix product state methods: To tangent space and beyond, Phys. Rev. B **88**, 075133 (2013).
[40] S.-C. T. Choi, C. C. Paige, and M. A. Saunders, MINRES-QLP: A Krylov subspace method for indefinite or singular symmetric systems, SIAM J. Sci. Comput. **33**, 1810 (2011).
[41] See Supplemental Material at http://link.aps.org/supplemental/10.1103/PhysRevB.102.165128 for details on time-dependent variational Monte Carlo; plot on the energy deposition; scaling of the charge structure factor; estimation of the Kondo temperature and the RKKY interaction; computation of the optical conductivity; and explanation on the computation of the high harmonic generation.
[42] P. J. W. Moll, B. Zeng, L. Balicas, S. Galeski, F. F. Balakirev, E. D. Bauer, and F. Ronning, Field-induced density wave in the heavy-fermion compound $CeRhIn_5$, Nat. Commun. **6**, 6663 (2015).
[43] E. Moshopoulou, J. Sarrao, P. Pagliuso, N. Moreno, J. Thompson, Z. Fisk, and R. Ibberson, Comparison of the crystal structure of the heavy-fermion materials $CeCoIn_5$, $CeRhIn_5$, and $CeIrIn_5$, Appl. Phys. A **74**, s895 (2002).
[44] M. Capello, F. Becca, M. Fabrizio, S. Sorella, and E. Tosatti, Variational Description of Mott Insulators, Phys. Rev. Lett. **94**, 026406 (2005).
[45] L. F. Tocchio, C. Gros, X.-F. Zhang, and S. Eggert, Phase Diagram of the Triangular Extended Hubbard Model, Phys. Rev. Lett. **113**, 246405 (2014).
[46] L. F. Tocchio, A. Montorsi, and F. Becca, Metallic and insulating stripes and their relation with superconductivity in the doped Hubbard model, SciPost Phys. **7**, 21 (2019).
[47] C. Shao, T. Tohyama, H.-G. Luo, and H. Lu, Numerical method to compute optical conductivity based on pump-probe simulations, Phys. Rev. B **93**, 195144 (2016).
[48] S. Ghimire, A. D. DiChiara, E. Sistrunk, P. Agostini, L. F. DiMauro, and D. A. Reis, Observation of high-order harmonic generation in a bulk crystal, Nat. Phys. **7**, 138 (2011).
[49] S. Ghimire and D. A. Reis, High-harmonic generation from solids, Nat. Phys. **15**, 10 (2019).
[50] F. H. M. Faisal and J. Z. Kamiński, Floquet-Bloch theory of high-harmonic generation in periodic structures, Phys. Rev. A **56**, 748 (1997).
[51] A. F. Kemper, B. Moritz, J. K. Freericks, and T. P. Devereaux, Theoretical description of high-order harmonic generation in solids, New J. Phys. **15**, 023003 (2013).
[52] G. P. Zhang, M. S. Si, M. Murakami, Y. H. Bai, and T. F. George, Generating high-order optical and spin harmonics from ferromagnetic monolayers, Nat. Commun. **9**, 3031 (2018).
[53] T. T. Luu and H. J. Wörner, High-order harmonic generation in solids: A unifying approach, Phys. Rev. B **94**, 115164 (2016).
[54] S. Ghimire, A. D. DiChiara, E. Sistrunk, G. Ndabashimiye, U. B. Szafruga, A. Mohammad, P. Agostini, L. F. DiMauro, and D. A. Reis, Generation and propagation of high-order harmonics in crystals, Phys. Rev. A **85**, 043836 (2012).
[55] Y. Murakami, M. Eckstein, and P. Werner, High-Harmonic Generation in Mott Insulators, Phys. Rev. Lett. **121**, 057405 (2018).
[56] N. Tancogne-Dejean, M. A. Sentef, and A. Rubio, Ultrafast Modification of Hubbard U in a Strongly Correlated Material: *Ab initio* High-Harmonic Generation in NiO, Phys. Rev. Lett. **121**, 097402 (2018).
[57] D. N. Basov, R. D. Averitt, and D. Hsieh, Towards properties on demand in quantum materials, Nat. Mater. **16**, 1077 (2017).
[58] Y. Mizukami, H. Shishido, T. Shibauchi, M. Shimozawa, S. Yasumoto, D. Watanabe, M. Yamashita, H. Ikeda, T. Terashima, H. Kontani, and Y. Matsuda, Extremely strong-coupling superconductivity in artificial two-dimensional Kondo lattices, Nat. Phys. **7**, 849 (2011).
[59] D. K. Pratt, W. Tian, A. Kreyssig, J. L. Zarestky, S. Nandi, N. Ni, S. L. Bud'ko, P. C. Canfield, A. I. Goldman, and

R. J. McQueeney, Coexistence of Competing Antiferromagnetic and Superconducting Phases in the Underdoped $Ba(Fe_{0.953}Co_{0.047})_2As_2$ Compound Using X-Ray and Neutron Scattering Techniques, Phys. Rev. Lett. **103**, 087001 (2009).

[60] T. Park, E. D. Bauer, and J. D. Thompson, Probing the Nodal Gap in the Pressure-Induced Heavy Fermion Superconductor $CeRhIn_5$, Phys. Rev. Lett. **101**, 177002 (2008).

[61] M. Heyl, A. Polkovnikov, and S. Kehrein, Dynamical Quantum Phase Transitions in the Transverse-Field Ising Model, Phys. Rev. Lett. **110**, 135704 (2013).

[62] S. Paeckel, B. Fauseweh, A. Osterkorn, T. Köhler, D. Manske, and S. R. Manmana, Detecting superconductivity out of equilibrium, Phys. Rev. B **101**, 180507 (2020).